Research

Author for correspondence:

K.L.P. Warburton

e-mail: klpw3@cam.ac.uk

Shear dilation of subglacial till results in time-dependent sliding laws

K. L. P. Warburton[1,2], D. R. Hewitt[3] and J. A. Neufeld[2,4,5]

[1]Thayer School of Engineering, Dartmouth College, Hanover, NH 03755 USA
[2]Department of Applied Mathematics and Theoretical Physics, University of Cambridge, Wilberforce Road, Cambridge CB3 0WA, UK
[3]Department of Mathematics, University College London, 25 Gordon Street, London, WC1H 0AY, UK
[4]Centre for Environmental and Industrial Flows, University of Cambridge, Madingley Rise, Cambridge CB3 0EZ, UK
[5]Department of Earth Sciences, Bullard Laboratories, University of Cambridge, Madingley Rise, Cambridge CB3 0EZ, UK

The dynamics of glacial sliding over water-saturated tills are poorly constrained and difficult to capture realistically in large scale models. Experiments characterise till as a plastic material with a pressure-dependent yield stress, but the subglacial water pressure may fluctuate on annual to daily timescales, leading to transient adjustment of the till. We construct a continuum two-phase model of coupled fluid and solid deformation, describing the movement of water through the pore space of a till that is itself dilating and deforming. By forcing the model with time-dependent effective pressure at the ice-till interface we infer the resulting relationships between basal traction, solid fraction, and rate of deformation. We find that shear dilation introduces internal pressure variations and transient dilatant strengthening emerges, leading to hysteretic behaviour in low-permeability materials. The result is a time-dependent effective sliding law, with permeability-dependent lag between changes in effective pressure and the sliding speed. This deviation from traditional steady-state sliding laws may play an important role in a wide range of transient ice-sheet phenomena, from glacier surges to the tidal response of ice streams.

1. Introduction

The fast-flowing ice streams and outlet glaciers of the Antarctic and Greenland ice sheets flow at rates several orders of magnitude faster than the slowly moving ice around them [1]. The majority of this speed difference is due to the much larger basal velocity of the ice in these regions, sliding over and inducing deformation in the weaker sediment below, known as subglacial till [2,3]. Since these ice streams control the majority of ice flow out of the ice sheets, understanding and modelling the processes occurring at the ice-till interface are of key importance in predicting the future dynamics of the Antarctic and Greenland ice sheets [4].

Compared to the bedrock below slower-flowing regions, till is a weaker material, comprised of water-saturated, clay-rich sand or pebbly mud. Water pressure variations in the pore space between grains strongly affects the bulk strength of the till, and the resistance it provides to the flow of the ice above. A key quantity for determining the ice dynamics is the effective pressure N, the difference between the ice overburden pressure and the pore water pressure. Many experiments have shown that till is well-described as a plastic material whose yield stress τ_b depends linearly on N through a roughly constant friction coefficient $\mu = \tau_b/N$ [3,5–7].

However, water pressure in the subglacial environment is not constant over time; it fluctuates on timescales from hourly (tidal forcing, daily surface melt) to yearly (summer melt season) to multi-decadal, accompanied by a response in the glacier surface speed [8–11]. Nor are these pressure changes necessarily spatially uniform [12,13]. Increasingly, observations [9], simulations [14,15], and experiments [16] have shown the potential for transient adjustment of basal dynamics to introduce hysteresis and lag between changes in effective pressure and changes in sliding speed, in settings dominated by either hard-bedded or soft-bedded sliding.

Sliding laws, which link traction at the ice-bed interface τ_b, subglacial effective pressure N, and the sliding speed of the ice u_b, are usually formulated in terms of steady-state values of these parameters [4,17,18]. Thus when these laws are incorporated into large scale models, an instantaneous relationship is assumed between changes in effective pressure and sliding speed. But when the changes in basal conditions occur on a timescale comparable to the transient adjustment of the till, we would also expect this transient drag to play an important role in setting the dynamics of ice flow [14,16].

It has long been noted [3,5] that acceleration after a decrease in effective pressure can lead to shear-driven dilation of the till. The consequent increase in pore space, transient change in pore pressure, and the accompanying increase in yield stress have been proposed as self-regulatory mechanisms that limit the impact of varying subglacial conditions on sliding speed. These 'dilant strengthening' phenomena are not observed in dry till, but are a transient feature in wet till, which suggests that pore-pressure variations and the associated flow of water play a key role in determining the till response [19]. The processes occurring in the till - grain rearrangement [20], induced water flow and pressure diffusion - take time, setting natural timescales for the transient response of the subglacial environment.

In this paper we construct a coupled model of till deformation, shear dilation, and the water flow through this changing environment. In the time-dependent case we track the flow of water in and out of the pore space and calculate the pressure gradients needed to drive this flow. We construct our model of the subglacial till from the simplest possible set of physically based equations, describing mass conservation and force balance to construct a general framework. For even simple forcing we show that complex behaviour emerges, without the need to resort to any ad-hoc parametrization. Within this setup we make use of newly derived continuum models of water-saturated granular rheology to model the response of subglacial till to transient forcing [14,21–23]. Similarly to [14] we observe diffusion of pressure fluctuations through the depth of the till in response to surface conditions, but we interpret this response in terms of changes in porosity and analytically predict the resultant sliding law. Recently, models for the transient evolution of basal traction based on a rate-and-state friction (RSF) framework have been applied
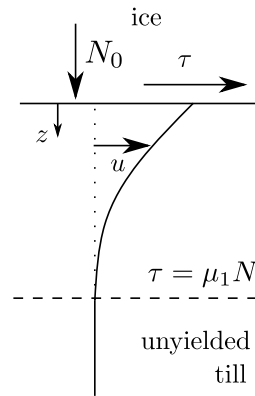
Figure 1. A diagram showing steady shear, indicating the notation used. Note z is depth from the ice-till interface (downwards).

to the dynamics of glacier beds [16,24,25]; we discuss this transient friction in terms of the pore-scale physics, to understand the link between the RSF parameter values and the characteristics of the subglacial till.

We verify that the steady-state deformation of the till predicted by our model is consistent with experimental results and field observations. We then use the time-dependent model to explore the impact of shear dilation on transient water pressure gradients within subglacial till, and the resulting relationship between basal traction, effective pressure, till solid fraction and deformation rate at the ice-till interface. We predict the amplitude and lag of the deformation in response to a range of frequencies of pressure forcing, allowing us to derive a time-dependent sliding law for a water-saturated deformable bed.

2. Governing equations and general set-up

In this study, we model the dynamic response of a deep layer of till to an imposed (possibly time-dependent) normal stress and shear stress applied at its surface. We assume that there is no variation of the system in the horizontal direction (thus neglecting larger-scale effects, such as ploughing of clasts), and that the solid fraction of the till being denser than water is the primary reason for vertical variation in till properties and dynamics.

We start by considering the equations for mass conservation and force balance within a one-dimensional slice of till. We take coordinate axes such that shear is applied in the x-direction, with the z-axis in the direction of gravity (figure 1). The subglacial till comprises of a solid granular matrix with density ρ_s, solid volume fraction ϕ, and which deforms continuously with velocity $\boldsymbol{v_s} = (u_s(z,t), 0, v_s(z,t))$, along with the water in the pore space, which correspondingly has density ρ_w and velocity $\boldsymbol{v_w} = (u_w, 0, v_w)$.

Tracking the movement of the grains, and hence the local solid mass, the solid fraction ϕ evolves as

$$\frac{\partial \phi}{\partial t} + \frac{\partial}{\partial z}(v_s \phi) = 0, \tag{2.1}$$

assuming that individual grains are incompressible. Conservation of water in the pore space, taking the water as incompressible, is given by

$$\frac{\partial(1-\phi)}{\partial t} + \frac{\partial}{\partial z}[v_w(1-\phi)] = 0, \tag{2.2}$$

and so total mass conservation is

$$\frac{\partial}{\partial z}[v_s \phi + v_w(1-\phi)] = 0. \tag{2.3}$$

Assuming that the till is sufficiently deep that there is a region where the grains are stationary, with no vertical water flow, this can be integrated to give

$$v_w = -\frac{\phi}{1-\phi} v_s, \tag{2.4}$$

although if there is a background vertical drainage of water through the full depth of the till, (2.4) could be modified by the inclusion of an additional flux.

Any flow of water through the pore space must be driven by a non-hydrostatic gradient in the pore water-pressure p_w, here described by Darcy's law for the flux of water,

$$-\frac{k}{\eta}\left(\frac{\partial p_w}{\partial z} - \rho_w g\right) = (1-\phi)(v_w - v_s). \tag{2.5}$$

Here η is the viscosity of water and $k(\phi)$ is the permeability of the till, which in general is a function of the solid fraction. Using (2.4) in (2.5) we have the simpler expression for the solid vertical velocity

$$\frac{k}{\eta}\left(\frac{\partial p_w}{\partial z} - \rho_w g\right) = v_s. \tag{2.6}$$

Within the till, force-balance requires that gravity be balanced by gradients in stress. Hence the divergence of the total stress tensor $\boldsymbol{\sigma}$ of the till is given by

$$\nabla \cdot \boldsymbol{\sigma} = -\left[\rho_s \phi + \rho_w(1-\phi)\right]\boldsymbol{g}. \tag{2.7}$$

The pore water pressure supports a portion of the stress on the till, and the effective stress tensor, $\boldsymbol{\sigma^e} = \boldsymbol{\sigma} + p_w \boldsymbol{I}$, is the remaining stress experienced by the granular matrix, which may cause deformation if exceeding the yield stress. From the force-balance equation (2.7), it is apparent that the normal stress increases with depth (increasing z), and is modulated by the pore water pressure,

$$\frac{\partial p_w}{\partial z} - \frac{\partial \sigma_{zz}^e}{\partial z} = \rho_w g + \Delta\rho\, g\phi, \tag{2.8}$$

where $\Delta\rho = \rho_s - \rho_w$. The horizontal shear stress is constant and the shear stress τ_b exerted at the ice-bed interface is transmitted uniformly down through the till,

$$\frac{\partial \sigma_{xz}^e}{\partial z} = 0 \quad \Rightarrow \quad \sigma_{xz}^e = \tau_b. \tag{2.9}$$

Combining (2.8) and (2.6), we see that vertical effective stress gradients in excess of the background hydrostatic pressure gradient drive compaction and vertical motion of the solid phase,

$$\frac{\eta}{k} v_s = \frac{\partial \sigma_{zz}^e}{\partial z} + \Delta\rho\, g\phi. \tag{2.10}$$

Thus to find the vertical solid velocity v_s that drives the evolution of the solid fraction via (2.1) we need to calculate the distribution of effective stress felt by the till, $\boldsymbol{\sigma^e}$, as a function of the stress applied at its surface and the instantaneous solid fraction ϕ. We anticipate that we must describe the rheology of the till, linking stress to velocity gradients and thus forming a differential equation for v_s, as well as the constitutive law for ϕ which determines its propensity to compact and create anisotropy in the stress field.

We define two useful quantities by decomposing the effective stress into an effective pressure $N = -\frac{1}{3}\left(\sigma_{xx}^e + \sigma_{yy}^e + \sigma_{zz}^e\right)$ and the deviatoric stress $\hat{\boldsymbol{\sigma}}$ according to $\boldsymbol{\sigma^e} = -N\boldsymbol{I} + \hat{\boldsymbol{\sigma}}$, with

$$\hat{\boldsymbol{\sigma}} = \begin{pmatrix} \sigma_{xx}^e + N & 0 & \tau_b \\ 0 & \sigma_{yy}^e + N & 0 \\ \tau_b & 0 & \sigma_{zz}^e + N \end{pmatrix}. \tag{2.11}$$

Similarly, we can decompose the shear rate $\boldsymbol{S}$ into a compaction (or dilation) rate $\partial v_s/\partial z$, and a deviatoric shear rate $\dot{\boldsymbol{\gamma}}$ via

$$\boldsymbol{S} = \begin{pmatrix} 0 & 0 & \frac{\partial u_s}{\partial z} \\ 0 & 0 & 0 \\ \frac{\partial u_s}{\partial z} & 0 & 2\frac{\partial v_s}{\partial z} \end{pmatrix} = \frac{2}{3}\frac{\partial v_s}{\partial z}\boldsymbol{I} + \dot{\boldsymbol{\gamma}}, \tag{2.12}$$

$$\dot{\boldsymbol{\gamma}} = \begin{pmatrix} -\frac{2}{3}\frac{\partial v_s}{\partial z} & 0 & \frac{\partial u_s}{\partial z} \\ 0 & -\frac{2}{3}\frac{\partial v_s}{\partial z} & 0 \\ \frac{\partial u_s}{\partial z} & 0 & \frac{4}{3}\frac{\partial v_s}{\partial z} \end{pmatrix}. \tag{2.13}$$

In this paper we restrict ourselves to considering isotropic materials for which the deviatoric stress and deviatoric shear rate are parallel, that is

$$\frac{\dot{\boldsymbol{\gamma}}}{\dot{\gamma}} = \frac{\hat{\boldsymbol{\sigma}}}{\hat{\sigma}}, \tag{2.14}$$

where non-bold symbols denote the magnitude of a tensor, $M = |\boldsymbol{M}| = \sqrt{\frac{1}{2}(M_{ij}M_{ij})}$. By comparing components, we see that $\sigma_{xx}^e = \sigma_{yy}^e$, and

$$\hat{\sigma} = \sqrt{\tau_b^2 + \frac{3}{4}(\sigma_{zz}^e + N)^2}, \tag{2.15}$$

$$\dot{\gamma} = \sqrt{\frac{\partial u_s}{\partial z}^2 + \frac{4}{3}\frac{\partial v_s}{\partial z}^2}. \tag{2.16}$$

A plastic material has a yield stress below which no flow occurs, and for which additional applied shear stress above the yield stress results in increasing amounts of deformation. The yield stress of till has been widely observed to depend linearly on its effective pressure [3,6], so we expect a yield condition of the form $\hat{\sigma} = \mu_1 N$. Hence in general we can write the rheology of a yield-stress till as

$$\dot{\gamma} = \begin{cases} \dot{\gamma}(\hat{\sigma}, N) & \hat{\sigma} > \mu_1 N, \\ 0 & \hat{\sigma} < \mu_1 N, \end{cases} \tag{2.17}$$

where μ_1 is a static friction coefficient, with $\mu_1 \sim 0.5$ for till [6]. We expect the shear rate to increase with shear stress, $\partial\dot{\gamma}/\partial\hat{\sigma} > 0$, and decrease with effective pressure (since the yield stress increases) so $\partial\dot{\gamma}/\partial N < 0$. If the shear stress is close to the yield stress, the general leading-order form of the shear rate will have some power-law dependence $\dot{\gamma} = C(\hat{\sigma} - \mu_1 N)^a$ on this stress difference.

To evolve the porosity by (2.1), the solid velocity v_s needs to be calculated as a function of ϕ only. Thus we need an expression for $\partial\sigma_{zz}^e/\partial z$ in (2.10). By combining (2.14) with a generalised rheology (2.17), the dilation (or compaction) rate during shear is

$$\frac{\partial v_s}{\partial z} = \frac{3\dot{\gamma}}{4}\frac{\sigma_{zz}^e + N}{\hat{\sigma}(\dot{\gamma}, N)}, \tag{2.18}$$

meaning that if $\dot{\gamma}$ and N can be determined in terms of σ_{zz}^e and ϕ only, (2.18) and (2.10) can be combined to give a second-order differential equation for $v_s(\phi)$.

Since τ_b is constant in space, we can use the definition of $\hat{\sigma}$ (2.15) and the rheology (2.17) to write $\dot{\gamma} = \dot{\gamma}(\sigma_{zz}^e, N)$. Thus all that is needed to close the system is a constitutive law relating the solid fraction to local values of effective pressure and shear rate,

$$\phi = \phi(\dot{\gamma}, N). \tag{2.19}$$

On substituting for $\dot{\gamma}(\sigma_{zz}^e, N)$ this equivalently provides an expression for effective pressure of the form $N = N(\sigma_{zz}^e, \phi)$. Models based on critical state solid mechanics would assume that the solid fraction depends only on N, which simplifies this final step to $N = N(\phi)$. However, since it is readily included in this framework, we leave open the possibility of shear-rate dependence. Lower packing fraction at higher $\dot{\gamma}$ is observed in tills [26,27] and granular flows [21]. As we shall

show, shear-dilatancy of this form alters the strength of the induced water-pressure perturbations and the timescale of the transient response.

These governing equations describe the response of the till to the conditions at the ice-till interface, and in general can be forced by changes in effective pressure, shear stress or sliding speed. Solving these equations, we can calculate the transient response of the depth profiles of effective pressure, and we can then determine the shear rate, depth of the shear zone, surface speed, compaction rate, and solid fraction of the till. Here we will restrict our attention to the effect of changing effective pressure on surface speed when basal traction is kept constant, but other types of forcing can be analysed similarly.

This general set-up can be used to model a wide range of materials and produce a variety of behaviours. To model a specific scenario, we need to impose a constitutive relationship for the rheology (2.17) of the solid phase and the form of the solid fraction (2.19). In section 3 we shall show the results for a specific choice of constitutive laws, but for the rest of this section we discuss general behaviour resulting from this formulation.

(a) Steady state deformation and the diffusive limit of pressure variations

The extent to which till deforms in response to the stress exerted on it by the ice above depends on the shear rate throughout the deforming region, and the depth of the deforming region itself. The depth of the deforming region can be much shallower than the available depth of till, and this depth emerges as a result of the forcing at the ice-till interface [28]. Unless there is some shallow immovable layer on which the till rests, the depth to which it deforms is an important part of setting the sliding law and till transport.

In steady state, the till is neither compacting nor dilating and so $v_s = 0$. Thus by (2.14) the effective pressure is $N = -\sigma_{zz}^e$, the shear stress $\hat{\sigma} = \tau_b$, and therefore (2.10) indicates that N simply increases with depth through the till. Hence the yield strength of the till $\mu_1 N$ also increases, until it exceeds the shear stress τ_b applied by the ice.

From (2.10) the effective pressure N increases from its value N_0 at the ice-till interface as

$$N(z) = N_0 + \int_0^z \Delta\rho\, g\phi \; dz. \tag{2.20}$$

If ϕ remains close to a maximum value ϕ_m, we have $N \approx N_0 + \Delta\rho\, g\phi_m z$, and this depth-dependence naturally defines the depth of the yield surface [14,29] as

$$z_0 \approx \frac{\tau_b - \mu_1 N_0}{\mu_1 \Delta\rho\, g\phi_m}. \tag{2.21}$$

In the deforming region above this depth, (2.17) gives the shear rate, and so the flow rate of till is given by

$$u_s(z) = \int_z^{z_0} \dot{\gamma}(\tau_b, N_0 + \Delta\rho\, g\phi_m Z) \; dZ. \tag{2.22}$$

This equation can used to constrain the rheology of the till given a depth-profile of deformation. Taking as before the general power-law form for the leading-order behaviour of the shear rate when the yield stress is exceeded, $\dot{\gamma} = C(\hat{\sigma} - \mu_1 N)^a$ in (2.17), then

$$u_s(z) = \int_z^{z_0} C\left[\tau_b - \mu_1(N_0 + \Delta\rho\, g\phi_m Z)\right]^a \; dZ = \frac{C(\mu_1 \Delta\rho\, g\phi_m)^a}{a+1}(z_0 - z)^{a+1}, \tag{2.23}$$

and the total till flux is

$$u_s(z) = \int_0^{z_0} u_s(z) \; dz = \frac{C(\mu_1 \Delta\rho\, g\phi_m)^a}{(a+1)(a+2)} z_0^{a+2}. \tag{2.24}$$

Thus the surface of the till moves with speed

$$u_b = \frac{C(\tau_b - \mu_1 N_0)^{a+1}}{(a+1)\mu_1 \Delta\rho\, g\phi_m}. \tag{2.25}$$

If we neglect slip between the surface of the till and the bed of the ice, and thus interpret u_b as the sliding speed of the ice, we can invert for the traction law

$$\tau_b = \mu_1 N_0 + \left[\frac{(a+1)\mu_1 \Delta\rho\, g\phi_m}{C} u_b \right]^{1/a+1}, \tag{2.26}$$

where the second term is a small strengthening away from $\tau_b = \mu N_0$, regularising the speed while allowing for close-to-plastic behaviour.

In the limit of small perturbations about this steady state, the changes in porosity are small and flow is nearly horizontal, so $\sigma_{zz}^e \approx -N$, which greatly simplifies (2.10) so that (2.1) becomes a diffusion equation for changes in effective pressure,

$$\frac{d\phi}{dN} \frac{\partial N}{\partial t} = \frac{k\phi}{\eta} \frac{\partial^2 N}{\partial z^2}. \tag{2.27}$$

Since changes in solid fraction with effective pressure may generally be written as

$$\frac{d\phi}{dN} = \frac{\partial\phi}{\partial N} + \frac{\partial\phi}{\partial\dot\gamma} \frac{\partial\dot\gamma}{\partial N}, \tag{2.28}$$

the diffusion coefficient is

$$D = \frac{k}{\eta\alpha}, \tag{2.29}$$

with compressibility

$$\alpha = \alpha_0 + \alpha_{\dot\gamma} = \frac{1}{\phi} \frac{\partial\phi}{\partial N} + \frac{1}{\phi} \frac{\partial\phi}{\partial\dot\gamma} \frac{\partial\dot\gamma}{\partial N}. \tag{2.30}$$

The static compressibility of the till $\alpha_0 = \frac{\partial\phi/\partial N}{\phi}$ is augmented by a shear dilatancy $\alpha_{\dot\gamma} = \frac{1}{\phi} \frac{\partial\phi}{\partial\dot\gamma} \frac{\partial\dot\gamma}{\partial N}$. The reduction of the diffusion coefficient compared to the non-shearing case can therefore result in longer-lasting transient dynamics.

(b) Transient dynamics

Changes to the conditions at the ice-till interface alter the shear rate and drive the steady solid fraction towards a more dilated or compacted equilibrium. But in water-saturated till, the pore space is filled with water, so to achieve this new steady state with an altered volume of pore space, water must be driven through the till by non-hydrostatic pore-pressure gradients, which in turn affect the strength of the till and the shear rate at depth. This continues until a new steady-state balance is achieved between the surface forcing and the profiles of shear and solid fraction in the till, when the pore pressure is once again hydrostatic.

From the effective pressure evolution described in (2.27), given the total depth of the shear layer (2.21), the timescale for this process is

$$T \sim \frac{z_0^2}{D} \sim \frac{\eta\alpha(\tau_b - \mu_1 N_0)^2}{k(\mu_1 \Delta\rho\, g\phi_m)^2}. \tag{2.31}$$

The key parameters in setting this equilibration timescale are the permeability of the till k, the water viscosity η, and the till compressibility α. Since pressure gradients are inversely proportional to k, very permeable till will re-equilibrate rapidly, while very impermeable tills take so long to respond that the solid fraction appears almost fixed and the induced pressure gradients persist, not allowing the till to accelerate. The dependence on η provides a partial explanation for the vastly different response of dry till to transient forcing. Since air has much lower viscosity than water, the induced pressure gradients are much smaller, and the transient response is almost instantaneous in dry granular media. If k and η are known for a sample of till, measuring the timescale for re-equilibration following a step-change in forcing provides a way to constrain α.

When the surface shear rate increases and the till dilates, water is sucked into the till by decreasing the pore pressure at depth, increasing the effective pressure and strengthening the till. This is a negative feedback that transiently limits the shear rate. Conversely, when the surface

shear rate decreases and the till compacts, the water forced out of the pore space supports more of the weight of the ice and keeps the till flowing. In low permeability tills, the induced transient pressure gradients can be very large, even for small compaction rates.

(c) Periodic sliding law

Many processes providing water to the subglacial environment are periodic or quasi-periodic in nature, including pressure variations due to daily surface melt cycles or from tidal forcing propagating up from the grounding line. Glaciers also accelerate and decelerate over the same timescales, suggesting a link between variations in subglacial water availability and surface velocities modulated by changes in the basal traction [9,11,30]. Classical sliding laws assume an instantaneous relationship between effective pressure and sliding speed. We have described how dilatancy can introduce a time dependence, or lag, between the pressure forcing and the velocity response and that induced water pressure gradients can buffer the till at depth from the imposed pressure fluctuations. In this section we explore the response of water-saturated till to periodic fluctuations in effective pressure and examine the effect on the sliding law for a range of forcing frequencies and till permeabilities.

For simplicity, we consider a periodic sinusoidal forcing in effective pressure applied at the ice-till interface, while maintaining a fixed basal shear stress. When the amplitude of the pressure forcing is small, the governing equations may be linearised and analytic expressions for both the phase lag and relative amplitude of the velocity response (compared to steady state) can be calculated.

If the forcing is sufficiently slow compared to (2.31), the till is able to dilate or contract throughout the depth of the deforming region, and the pore pressure can equilibrate relatively rapidly. The transient effects happen on a timescale that is short compared to the forcing, so we recover an almost instantaneous sliding law, with the basal speed responding to every change in effective pressure. In contrast, if the frequency of the forcing is rapid the till cannot respond throughout the depth of the shear layer. The induced pore water pressure persists and counteracts the forcing, and the result is a sliding law that only depends on the average effective pressure, filtering out the fluctuations.

If the pressure forcing is

$$N_0 = \bar{N} + \Delta N e^{-i\omega t} \tag{2.32}$$

with $\Delta N \ll \bar{N}$ and taking the real part is implied, then the leading-order response is controlled by the diffusion equation (2.27). Given the linearity of the response to small variations, the surface velocity response takes the form

$$u_s(0,t) = u_b(\bar{N}) + \hat{u} = u_b(\bar{N}) + A \frac{du_b}{dN} \Delta N e^{-i(\omega t - \theta)}, \tag{2.33}$$

where A is the relative amplitude and θ is the phase lag. For quasi-instantaneous behaviour at low frequencies, $A \to 1$ and $\theta \to 0$. Induced pressure perturbations act to decrease the amplitude A (buffering the till from rapid fluctuations) and increase the phase lag θ.

To find A and θ, we solve (2.27) with (2.32) as a boundary condition, and find that the perturbation to N is given by $\hat{N} = \Delta N e^{-\lambda z - i\omega t}$ with $D\lambda^2 = -i\omega$. Again using the leading order form of the shear rate in (2.17) of $\dot{\gamma} = C(\tau_b - \mu_1 N)^a$, the perturbation to the shear rate becomes

$$\hat{\dot{\gamma}} = Ca \left[\mu_1 \Delta \rho \, g \phi_m (z_0 - z) \right]^{a-1} \mu_1 \Delta N e^{-\lambda z - i\omega t}. \tag{2.34}$$

Thus integrating from the static base of the shear layer to the surface implies that the perturbation to the surface velocity takes the form

$$\hat{u} = \left(\frac{a}{z_0^a} \int_0^{z_0} (z_0 - z)^{a-1} e^{-\lambda z} \, dz \right) \frac{du_b}{dN} \Delta N e^{-i\omega t}. \tag{2.35}$$

and the amplitude and lag of the velocity response are therefore

$$Ae^{i\theta} = a \int_0^1 (1-x)^{a-1} e^{-\lambda z_0 x} \, dx. \tag{2.36}$$

A clear transition appears when the timescale of dilatancy is small compared to the period of the pressure fluctuations $T = 2\pi/\omega$, or equivalently the perturbation reaches a depth comparable to that of the shear layer, when $\lambda z_0 \sim 1$. The transition frequency is thus given by

$$\omega \sim \frac{D}{z_0^2} \sim \frac{k(\mu_1 \Delta\rho \, g \phi_m)^2}{\eta\alpha(\tau_b - \mu_1 \bar{N})^2} \sim \frac{k}{\eta\alpha} \left[\frac{C(\mu_1 \Delta\rho \, g \phi_m)^{a/2}}{u_b} \right]^{2/(a+1)}. \tag{2.37}$$

In the limit of rapid perturbations, $\lambda z_0 \gg 1$ and the rapid fluctuations diffuse through the top of the till only before decaying. Equation (2.35) therefore reduces to

$$\hat{u} = \frac{a}{\lambda z_0} \frac{du_b}{dN} \Delta N e^{-i\omega t} = \frac{a\mu_1 \Delta\rho \, g \phi_m}{\tau_b - \mu_1 \bar{N}} \sqrt{\frac{k}{\omega\eta\alpha}} \frac{du_b}{dN} \Delta N e^{-i(\omega t - \pi/4)}, \tag{2.38}$$

which corresponds to a maximal phase lag of $\pi/4$, and an amplitude that depends on $\sqrt{k/\omega}$. The deformation lags behind the pressure forcing by a time $T/8$, which is linear in the period of forcing.

For slow perturbations with $\lambda z_0 \ll 1$, the perturbation makes it to the base of the shear layer, and we instead recover exactly the linearised form of the steady-state sliding law, as

$$Ae^{i\theta} = 1 - \frac{\lambda z_0}{a} + O\left((\lambda z_0)^2\right), \tag{2.39}$$

so $A \to 1$ and $\theta \sim \sqrt{\omega} \to 0$. The till responds to every change in effective pressure through the full depth of the till in this limit. The time lag continues to grow with the period of forcing, but now only like $\sqrt{T}$.

The transition frequency described by (2.37) is strongly dependent on the permeability, which is to be expected since lower values of till permeability require larger pressure gradients to drive the same amount of flow according to Darcy's law. This strengthens the buffering effect, and allows the till to act as a filter against high frequency variations in water pressure. By contrast, in high permeability tills, small induced pressure gradients equilibrate nearly instantaneously, and the response of the till mirrors the forcing.

3. Calculations with a granular rheology

To explore the behaviour of our coupled two-phase model in more detail, and extend it beyond the linear regime, we need to impose constitutive laws for $\dot{\gamma}(\hat{\sigma}, N)$ and $\phi(\dot{\gamma}, N)$. A granular rheology provides an attractive starting point for modelling the flow of a sample of till comprised largely of grains. Several key properties of till are also observed in granular media: nearly plastic behaviour with a pressure-dependent yield stress, shear dilation, and rapid flow once the yield stress is exceeded.

The granular literature defines two non-dimensional numbers which parametrise the rheology of granular flows. In granular media where grain-grain friction provides the dominant resistance to flow, the inertial number

$$I = \frac{\dot{\gamma}d}{\sqrt{N/\rho_s}}, \tag{3.1}$$

where d is the grain diameter, determines both $\hat{\sigma} = \mu(I)N$ and $\phi = \phi(I)$. This fits readily into the general framework introduced above since $I = I(\dot{\gamma}, N)$, and has been used by [14,29] to describe the rheology of till. However, in situations where the pore fluid modulates the inter-granular friction, we would expect the appropriate dimensionless scaling of the shear rate to instead be

given by the viscous inertial number

$$I_\nu = \frac{\eta \dot{\gamma}}{N}. \tag{3.2}$$

A transition between the two regimes occurs when $I^2 \sim I_\nu$ [31]. For the values of these parameters relevant to subglacial till (table 1), we have $I^2 \ll I_\nu \ll 1$, implying that the viscous scaling is dominant. The leading-order form of the experimentally measured $\mu(I_\nu)$ rheology [22] is

$$\mu = \mu_1 + M\sqrt{\frac{\eta \dot{\gamma}}{N}}, \tag{3.3}$$

where μ_1 is the static friction coefficient, and M is a constant describing the rate-dependence of the material after yield. Thus we can invert for the shear rate

$$\dot{\gamma} = \frac{1}{\eta M^2} \left(\hat{\sigma} - \mu_1 N \right)^2 N^{-1}. \tag{3.4}$$

The inertial-number dependent form of the solid fraction proposed by the same experiments is $\phi(I_\nu)$,

$$\phi = \frac{\phi_m}{1 + b\sqrt{\frac{\eta \dot{\gamma}}{N}}}. \tag{3.5}$$

It should be noted that subglacial inertial numbers are much lower than the values achieved in the mono-disperse granular experiments. However, [32] showed from DEM simulations that ϕ does continue to be a function of inertial number even in the near-static regime. This form of ϕ loses dependence on N when $\dot{\gamma} = 0$, in contrast to a critical-state packing fraction $\phi(N)$, which conversely has no dependence on $\dot{\gamma}$. While a transitional form of ϕ between critical state and inertial of the form $\phi_s(N) - f(I)$ has been suggested [33], given the lack of data to constrain a model of this form for till and since the general dynamics depend to leading order only on the total compressibility α, here we only show examples calculated using (3.5). In this case, the compressibility in (2.30) is

$$\alpha = \alpha_0 + \alpha_{\dot{\gamma}} = \frac{b\mu_1}{\tau_b}\sqrt{\frac{\eta \dot{\gamma}}{N}} + \frac{b\mu_1^2}{\tau_b M} \tag{3.6}$$

and the shear-dilatancy ($\alpha_{\dot{\gamma}}$) dominates over the static compressibility (α_0) at subglacial values of shear rate and effective pressure.

In steady state, since N increases with depth as given by (2.20), we obtain profiles for the shear rate and solid fraction with depth. To leading order in the inertial number these reduce to

$$\dot{\gamma} \approx \frac{N_0}{\eta} \left(\frac{\tau - \mu_1 N_0 - \mu_1 \Delta\rho\, g \phi_m z}{M N_0} \right)^2, \tag{3.7}$$

$$\phi \approx \phi_m \left(1 + \frac{\tau - \mu_1 N_0 - \mu_1 \Delta\rho\, g \phi_m z}{M N_0} \right)^{-1}, \tag{3.8}$$

as shown in figure 2.

Integrating through the yielded region we find that the speed of the till at the ice-till interface, $u_b = u_s(0)$, recovers a power law relationship between the sliding speed, driving stress, and effective pressure. This can equivalently be expressed as a traction law,

$$\tau_b = \tau(u_b) = \mu_1 N_0 + (3\eta\mu_1 \Delta\rho\, g \phi_m M^2 u_b N_0)^{1/3}, \tag{3.9}$$

This forms a granular equivalent to, or physical justification for, commonly used basal traction laws for ice sheet models, regularising the sliding speed while allowing for close to plastic behaviour. Perhaps unsurprisingly, the traction is dominated by the first, plastic, term since the rate-strengthening second term is typically only a very small correction given the relative sizes of u_b and N_0 in subglacial settings (figure 3c).
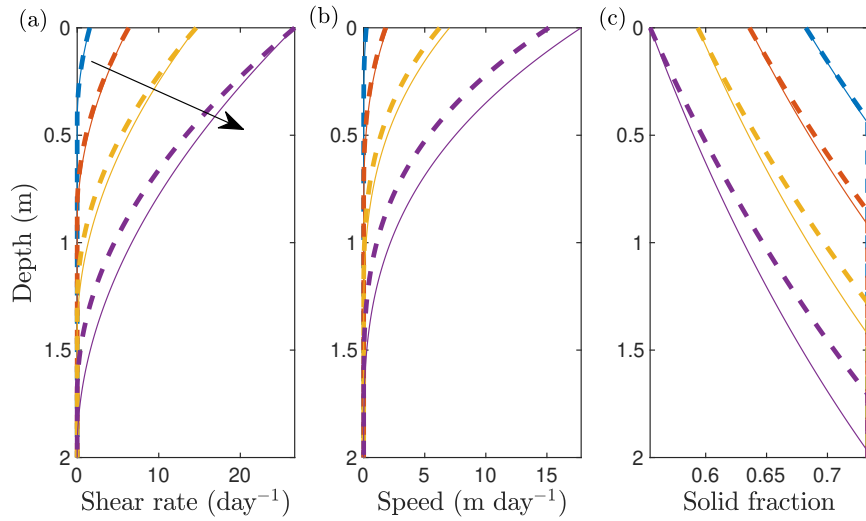
Figure 2. Steady-state profiles of (a) shear $\partial u_s / \partial z$, (b) horizontal speed u_s, and (c) solid fraction ϕ for different values of effective pressure, with $\tau_b - \mu_1 N_0 = 0.25, 0.5, 0.75, 1$ kPa increasing in the direction of the arrow. Solid lines show numerically calculated profiles, while dashed lines show the leading order expressions given in (3.7-3.8,3.11). The agreement is particularly good for low shear rates, as the leading order approximation is valid for small I_ν.

The total till flux can be found by integrating once more through the deforming region, and we find that to leading-order the steady-state till flux is

$$q_s = \frac{\phi_m}{12\eta(\mu_1 \Delta\rho \, g\phi_m M)^2} \frac{(\tau_b - \mu_1 N_0)^4}{N_0}. \tag{3.10}$$

Constraining the till flux is important for estimates of glacial erosion rates, and therefore setting the coupling between ice dynamics and subglacial topography that builds a wide array of bedforms. Understanding how ice sheet behaviour results in bedform construction can be used to interpret the topographic record of paleolithic ice streams, and exploit features from below current ice sheets to constrain till rheology.

(a) Fit to observations

The majority of experimental data on the deformation of subglacial till comes from ring-shear tests on thin layers of till, so the effective pressure and shear rate are close to uniform across the shearing region. This allows for comparison of the local form of μ as a function of N and $\dot{\gamma}$, but not the depth profiles. The conclusion from ring shear tests is that $\mu \approx 0.5$ and that this value is insensitive to the shear rate or effective pressure (see [6] for compiled data from 7 different ring shear tests). While our traction law is consistent with this conclusion, in that μ changes by only a few percent over speeds of up to kilometres per year (figure 3c), the lack of sensitivity means this steady-state data does not place a strong constraint on many of our model parameters.

It is perhaps more informative to look at in-situ deformation profiles from subglacial till samples. Using a granular rheology (3.3) in (2.23) we predict a velocity profile

$$u_s \approx \frac{M}{3\eta\mu_1 \Delta\rho \, g\phi_m} \left(\frac{\tau_b - \mu_1 N_0 - \mu_1 \Delta\rho \, g\phi_m z}{M N_0} \right)^3. \tag{3.11}$$

The depth of shear zones under glaciers has been observed to range from centimetres to metres [4,6,27]. Shear zone depths of this magnitude can be estimated from (2.21), the parameters of which are well constrained, and require that the traction difference $\tau_b - \mu_1 N_0 \approx 1$kPa. Since
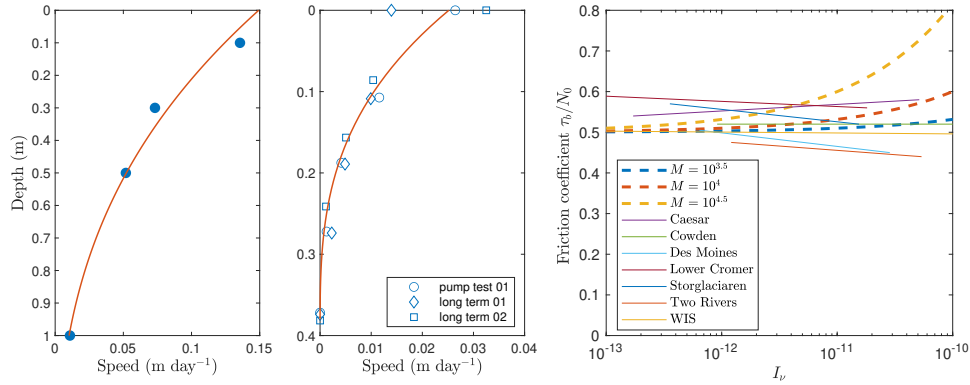
Figure 3. In-situ depth profiles (blue symbols) from (a) [34] and (b) [35] are well matched by the theoretical profiles (red lines) for $M = 10^{4.5}$ and $M = 10^{3.5}$ respectively. (c) The resulting traction law only deviates slightly from perfectly plastic even for large values of M, comparable to laboratory results from [6] (converted from $\dot{\gamma}$ to I_ν using reported pressures).

Parameter	Symbol	Value	Units
Fluid viscosity	η	1.8×10^{-3}	$\mathrm{kg\,m^{-1}s^{-1}}$
Density difference	$\Delta\rho g$	1.6×10^{3}	$\mathrm{kg\,m^{-2}s^{-2}}$
Till permeability*	k	$10^{-11} - 10^{-19}$	$\mathrm{m^2}$
Surface shear	τ_b	10^{4}	$\mathrm{kg\,m^{-1}s^{-2}}$
Static friction	μ_1	0.5	-
Friction parameter	M	10^{4}	-
Dilatancy parameter	b	5×10^{4}	-
Maximum solid fraction	ϕ_m	0.733	-

Table 1. Parameters values used in the numerical model. *Unless otherwise stated, $k = 10^{-12}\mathrm{m^2}$ is used.

the speed of till deformation is so low, (3.11) implies a large value of M, in contrast with experiments on idealised mono-disperse granular media where $M \sim 1$. In-situ measurements of till displacement with depth [34,35] show good agreement with our steady-state profiles if we take $M \sim 10^4$ (figures 3a and 3b). This suggests that once yielded, subglacial till has a much higher resistance to flow than the mono-disperse smooth grains typical of granular experiments. As well as geometric differences in the grains, a possible reason for this large resistance is that the clasts may experience an effective viscosity much larger than that of water, due to the high clay content in the soil, which would alter the appropriate scaling for the viscosity in the inertial number.

Finally we must constrain b, or equivalently α, using porosity variation with both $\dot{\gamma}$ and N. The static compressibility of clay-rich soils is on the order of $10^{-6} - 10^{-8}\mathrm{Pa^{-1}}$ [36], and experiments on till samples [3] at fixed shear rate and varying N confirm $\alpha_0 \sim 10^{-7}$. By contrast, in-situ profiles of porosity [27] in which $\dot{\gamma}$ and N both vary with depth are consistent with $b \sim 10^4$ and a much larger shear dilatancy of $\alpha_{\dot{\gamma}} \sim 10^{-4}\mathrm{Pa^{-1}}$. As noted for M, the value obtained for b is large in comparison with previous granular experiments and may point to a higher effective viscosity η of the interstitial fluid, increasing the sensitivity of μ and ϕ to the shear rate $\dot{\gamma}$. Fortunately, since b and M are both inversely proportional to the value of η used, our estimate of $\alpha \sim b/M$ remains independent of this uncertainty in effective viscosity and we can be confident that our numerical results capture a physically relevant regime for the transient response. The parameters used in the numerical model are given in table 1.

To better constrain all the parameters of this model would require further steady and time-dependent experiments on till. A systematic series of steady-state experiments on wet till would
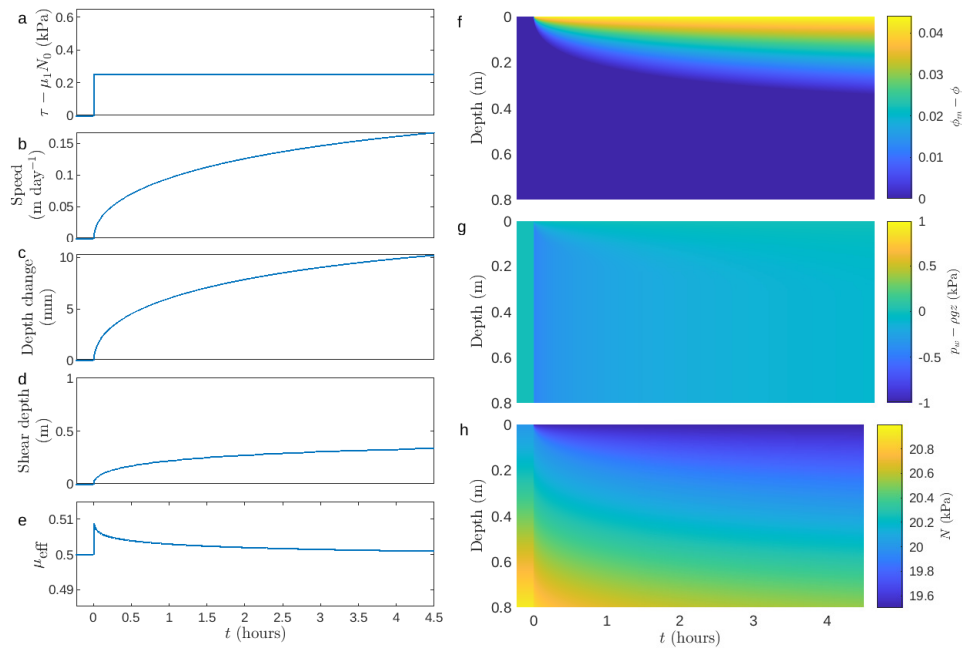
Figure 4. Behaviour of the system when the effective pressure at the surface is instantaneously decreased from $N = \tau_b/\mu_1$ to $N = 0.975\tau_b/\mu_1$, with an initially fully compacted till. Plots show (a) the forcing $\tau_b - \mu_1 N_0$, (b) surface velocity response $u_s(0)$, (c) increase in column height as the till decompresses, (d) depth of the yield surface, and (e) effective friction coefficient μ_{eff}. Depth profiles show (f) deviation from maximum solid fraction $\phi_m - \phi$, (g) pore water pressure deviation away from hydrostatic $p_w - \rho g z$, and (h) effective pressure N.

determine the applicability of wet granular models to till at low inertial number, and verify the appropriate steady-state values of M and b. In particular, the model predicts a large increase in α, and decrease in diffusivity, associated with even small amounts of shear-driven dilation, and further experiments to explore this prediction would be highly valuable. Furthermore, to assess the transient response of granular till, periodic experiments could be conducted to measure the depth and frequency dependence of the response. Such experimental investigations would provide invaluable insight into the time-dependent rheology of subglacial till, and would be a robust test of granular models of the deformation of wet till.

The details of the dynamic rheological behaviour of till may have important implications for the large-scale response of ice sheets to changes in basal conditions. In particular, granular till models exhibit a wide range of behaviours such as dilatant strengthening, compaction, persistent shear at depth, and sudden jamming, all of which may present as a frequency-dependent effective sliding law.

(b) Dilatant strengthening

If the effective pressure at the surface is suddenly decreased (figure 4a), there is an instantaneous acceleration at the surface as the yield stress decreases (4b). However, the till at depth does not respond instantaneously. Instead, the decrease in effective pressure diffuses downwards through the till (4h), along with an associated increase in shear rate and decrease in solid fraction (4f). The sliding speed gradually increases towards the new equilibrium value. This transient response of the sliding speed can be interpreted as a transient increase in till strength. To quantify this
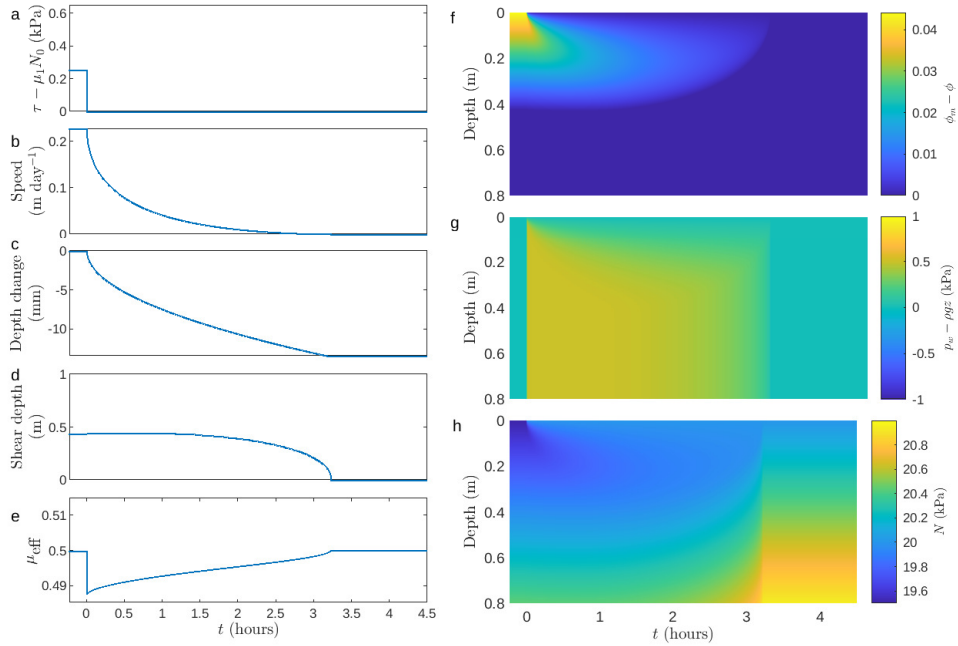
Figure 5. Behaviour of the system when the effective pressure at the surface is instantaneously increased from $N = 0.975\tau_b/\mu_1$ to $N = \tau_b/\mu_1$, with till porosity initially in steady state. Plots show (a) the forcing $\tau_b - \mu_1 N_0$, (b) surface velocity response $u_s(0)$, (c) decrease in column height as the till compresses, (d) depth of the yield surface, and (e) effective friction coefficient μ_{eff}. Depth profiles show (f) deviation from maximum solid fraction $\phi_m - \phi$, (g) pore water pressure deviation away from hydrostatic $p_w - \rho g z$, and (h) effective pressure N. The till fully jams at $t = 3.2$ hours.

strengthening, we use the steady-state traction law (3.9) to define an effective friction coefficient

$$\mu_{\text{eff}}(t, N_0) = \frac{\tau_b - [3\eta\mu_1 \Delta\rho\, g\phi_m M^2 u_s(0, t)N_0]^{1/3}}{N_0}. \tag{3.12}$$

Here, if the till deforms less than would be expected in steady state, $\mu_{\text{eff}} > \mu_1$, indicating dilatant strengthening.

To understand the mechanisms behind dilatant strengthening, we consider the non-hydrostatic component of the water pressure (figure 4g). As the till accelerates (figure 4b) and dilates (figure 4c), the expansion of the solid matrix induces a water pressure gradient that drives fluid into the increased pore space, lowering the pore water pressure at depth relative to hydrostatic. Despite the decrease in effective pressure at the surface, throughout most of the till the initial change in pore water pressure counteracts this surface change, and instead drives a strengthening of the till at depth (figure 4e). This introduces a lag between the surface forcing (figure 4a) and the response at depth (figure 4b), and hence a time dependence in the effective basal drag law, as illustrated by the effective friction coefficient, μ_{eff}, in figure (figure 4e).

(c) Compaction, shear at depth, and jamming

If the effective pressure at the surface is increased, there is a small instantaneous deceleration of the surface layer of the till, accompanied by compaction in this region. Similarly to the case of dilation, it takes time for the effective pressure at depth to increase as the pore water pressure re-equilibrates. The rate of deformation of the till therefore slowly decreases towards the new equilibrium value.

As the till compacts, water is driven upwards and out of the pore space by locally increased pore pressures at depth (figure 5g). Thus the effective pressure (5h), and the till strength (5e), are transiently lower than the new equilibrium. If the compaction is strong enough, the induced pore-pressure gradients can be sufficient to counteract the background hydrostatic gradient, leading to a decrease in effective pressure and till strength with depth (5h, early times). Thus the top layer of till can slide along over a layer of weaker material below, even if it is not itself deforming.

As the effective pressure at depth increases, the yield surface moves upwards (figure 5d). The till below the yield surface is fully compacted and stops deforming. As the overall rate of compaction decreases, less water is driven out of the pore space and so the strength of the pore water-pressure gradient is reduced. This increases the effective pressure, and the yield surface migrates further upwards through the till, reducing the zone of compaction further. This positive feedback can lead to a sudden shutdown of shear at depth as the till jams, as shown at late times in figure (5).

Given the rich dynamics of compaction compared to the gradual diffusion of pore pressure during dilation, this suggests that the system might exhibit complex hysteretic behaviour if the pressure oscillates. Indeed, that is exactly what we see in the case of large-amplitude periodic oscillations, as discussed in the following section.

(d) Periodic sliding law

The timescale for pressure diffusion and till compaction leads to the introduction of lag between the applied stress and deformation in the case of periodic forcing. With the introduction of an explicit rheology for the till, we can go beyond the linear calculation presented in section 2(c) and demonstrate the wealth of non-linear features emergent from the two-phase model, including periodic jamming and stick-slip motion in response to smoothly varying forcing.

To show first the linearised results, we take the pressure forcing to be periodic and sinusoidal, $N_0 = \bar{N} + \Delta N e^{-i\omega t}$, and use the granular rheology of (3.3) in the general formula for the amplitude and phase lag of the velocity response (2.36). This gives a velocity perturbation

$$\hat{u} = \frac{2\mu_1[\lambda(\tau_b - \mu_1\bar{N}) - \mu_1\Delta\rho\,g\phi_m(1 - e^{-\lambda z_0})]}{\lambda^2\eta M^2\bar{N}}\Delta N e^{-i\omega t} = A\frac{du_b}{dN}\Delta N e^{-i(\omega t - \theta)}, \qquad (3.13)$$

where $\lambda^2 = -i\omega/D$. These values of A and θ are shown in figure 6, and clearly show the transition that occurs when the timescale of dilatancy is small compared to the period of the pressure fluctuations,

$$\omega \sim \frac{D}{z_0^2} \sim \frac{k(\mu_1\Delta\rho\,g\phi_m)^2}{\eta\alpha(\tau_b - \mu_1\bar{N})^2} \sim \frac{k\mu_1^2(\Delta\rho\,g\phi_m)^{4/3}}{\eta^{5/3}\alpha M^{4/3}\tau_b^{2/3}u_b^{2/3}}. \qquad (3.14)$$

In the limit of rapid perturbations, $\lambda z_0 \gg 1$ and the rapid fluctuations diffuse through the top of till only before decaying. Equation (3.13) therefore reduces to

$$\hat{u} = \frac{2\mu_1(\tau_b - \mu_1\bar{N})}{\lambda\eta M^2\bar{N}}\Delta N e^{-i\omega t} = \frac{2\mu_1(\tau_b - \mu_1\bar{N})}{M^2\bar{N}}\sqrt{\frac{k}{\omega\eta^3\alpha}}\Delta N e^{i\pi/4 - i\omega t}, \qquad (3.15)$$

again showing the generic phase lag of $\pi/4$, and an amplitude that decreases as the frequency of oscillations increases, until the speed of the till depends only on the average value of the effective pressure. In effect, induced water-pressure variations buffer the till at depth from feeling the effect of surface changes.

Slow perturbations, with $\lambda z_0 \ll 1$, reach the base of the shear layer, and so the surface velocity of the till changes as

$$\hat{u} = \frac{\mu_1^2\Delta\rho\,g\phi_m z_0^2}{\eta M^2\bar{N}}\Delta N e^{-i\omega t} = \frac{(\tau_b - \mu_1\bar{N})^2}{\eta\Delta\rho\,g\phi_m M^2\bar{N}}\Delta N e^{-i\omega t} = \frac{du_b}{d\bar{N}}\Delta N e^{-i\omega t}, \qquad (3.16)$$

which is exactly the linearised form of the steady-state sliding law.
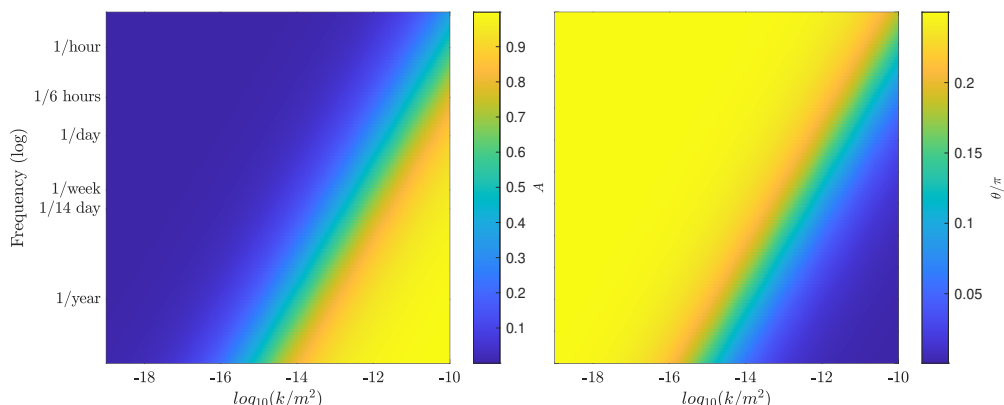
Figure 6. Analytically calculated values of (a) the relative amplitude of the velocity response compared to steady state A, and (b) the phase lag θ/π. Quasi-steady behaviour corresponds to $A = 1$ and $\theta = 0$, achieved for high permeability or low frequencies.

As shown in figures 7a and 7b, the till velocity is approximately constant in response to high frequency changes. As the frequency of forcing is decreased, the amplitude of the velocity response increases and the phase lag reduces, so that the response traverses the steady-state curve. This generic behaviour is seen both at small amplitudes (figure 7a), for which the above linearisation holds, and for much larger amplitudes of forcing (figure 7b) under which the velocity responds non-linearly. In both cases, it is the frequency of the fluctuation relative to the transition frequency (3.14) that determines whether the velocity response depends only on the average forcing, or is a quasi-instantaneous response following the steady-state sliding law. Between the two limits, the phase lag combined with the significant amplitude of the velocity response produces hysteresis loops, with sliding speeds remaining high during compaction, and low during dilation.

The hysteresis in the system is exaggerated if, during forcing, the effective pressure at the ice-till interface is high enough that $\tau_b < \mu_1 N_0$. For frequencies below the transition frequency, there is a smooth progression along the steady-state sliding law, with shear stopping when $N_0 > \tau_b/\mu_1$ and resuming when it crosses that value again. More complex behaviour emerges when the forcing is above the transition frequency, as rapid compaction can lead to an extented period of continued flow at depth, followed by jamming (see figure 8). Once jammed, shear cannot restart until the top layer of the till begins to yield again. Shear begins at the top of the till, and the yield surface then moves down. This highly asymmetric process between the shutdown and start up of shear gives a highly complex, stick-slip response of the till to simple periodic forcing.

4. Discussion

There are numerous instances where the transient response of ice sheets is important, from the rapid response to subglacial flooding events, the daily or annual variation of meltwater supply to the bed, and the sudden reduction in back-stress after the rapid disintegration of ice-shelves. To describe these scenarios requires a coupling of ice dynamics and basal processes. Here we focus on the response of ice streams to ocean tides, and comment on the relationship of the current work to rate-and-state models of transient ice-bed friction.

(a) Tidal response of ice streams

When applying this time-dependent sliding law to an ice stream model, the main distinction is whether the lag introduced by till dynamics is significant compared to the period of forcing, or
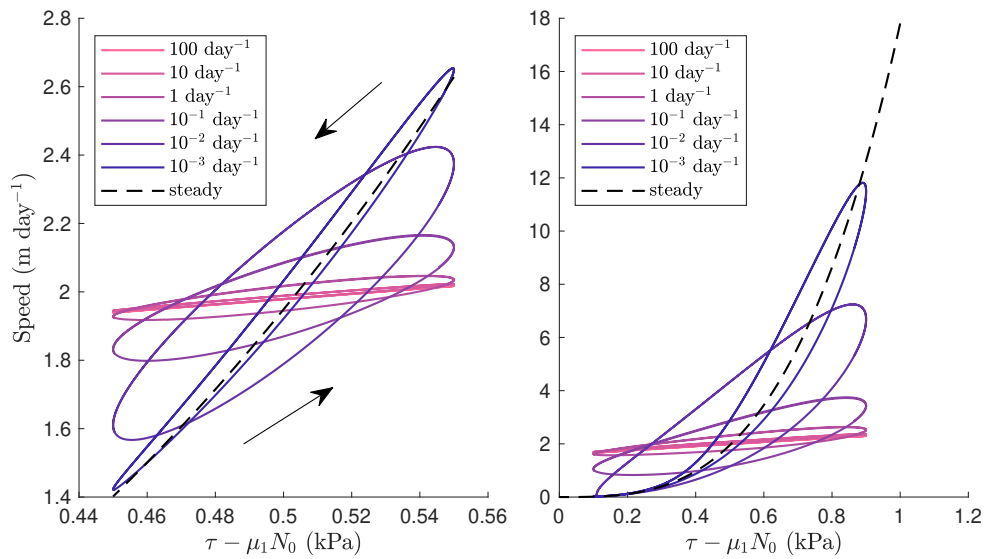
Figure 7. Till surface speed for fluctuating effective pressure - trajectories are traversed in the direction of arrows. (a) For small amplitude pressure perturbations, the velocity response is also sinusoidal, with some phase lag. As the frequency increases, the amplitude decreases. At low frequency the steady-state sliding law is recovered. (b) For larger amplitudes these trends are maintained, but there is a higher degree of hysteresis and the non-linear shape of the steady-state sliding law becomes apparent.
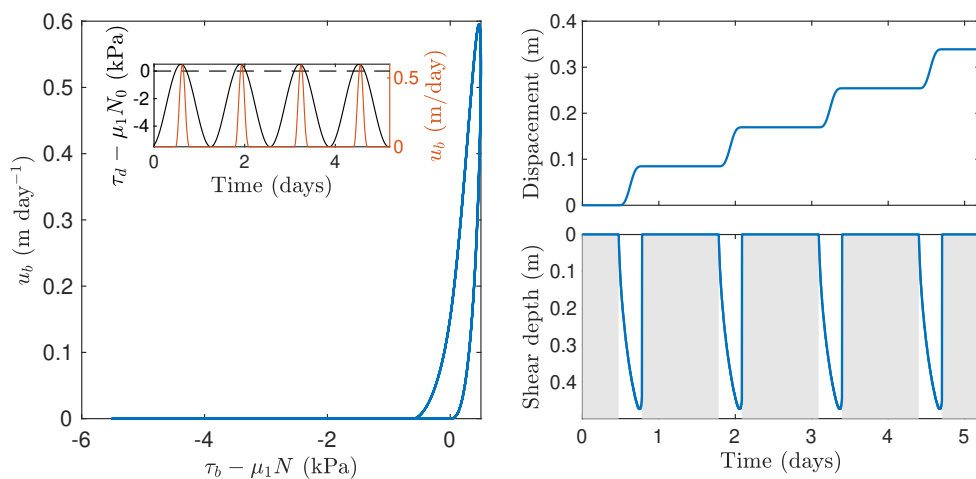

Figure 8. Slip-stick response of till to large and rapid sinusoidal pressure oscillations, showing the hysteresis in the surface velocity response to periodic changes in N, cumulative displacement of the till surface over several slip-stick cycles, and depth of the deforming region. Grey shading indicates times when the till is fully static.

whether an instantaneous sliding law remains appropriate. Since the velocity response to pressure changes is only significant when the frequency of changes is slower than the permeability-dependent transition frequency (2.37), this can be used as a constraint on the permeability of subglacial till.

At Rutford, despite the daily tidal forcing, the largest constituent of the velocity response is at the fortnightly frequency [37,38]. This model provides two possible mechanisms for this observation. The non-linearity of the till rheology may be sufficient to mix the daily frequencies and generate the fortnightly signal in-situ, similar to the suggestion of [39]. In the supplementary material we show the effect of forcing the model with two diurnal modes, and find that a weak fortnightly signal is generated in the sliding speed. Alternatively, if a fortnightly component is already present in the pressure signal before it reaches the upstream till, generated by the ice dynamics (for example at the grounding line) [40,41], then the dynamic response of the subglacial till may act as a low-pass filter, filtering out the daily signal and increasing the strength of the fortnightly component.

Indeed, one important lesson from this modelling of transient effects is that care should be taken when interpreting surface velocities as directly reflecting subglacial water pressures, both in the timing and the magnitude of their fluctuations. Because the local velocity signal lags behind the effective pressure, the time taken for glaciers to respond may not be the same as the time for the water to transit through the subglacial environment - this could explain the timing of slip events relative to the tidal cycle [11] or of the lag between borehole pressures and sliding speeds [42]. Similarly, since the adjustment of the till porosity can buffer the sliding speed against acceleration, inversions using an instantaneous sliding law may underestimate the magnitude of pressure changes driving velocity perturbations [30,43].

Considering the slip-stick motion of the Whillans Ice Stream, it is noteworthy that this continuum granular model is able to generate slip-stick cycles from a simple rheology, one that also produces continuously varying flow when the mean effective pressure is only slightly lower. This supports the view that the hydrology of the region results in the characteristic motion of the Whillans Ice Stream [3,44]. However, the inclusion of further details of the elastic ice response, which we have not modelled here, may be required to reproduce features such as secondary slip events at low tide [45]. Another mechanism not included here is the short-timescale elastic behaviour of the ice-till interface itself, which is known to generate seismic events and allow for rapid acceleration [44]. This model is far from a complete description of the Whillans slip events, but does show how intermittent sliding can result from a continuum model.

(b) Comparison to the rate-and-state friction framework

The rate-and-state friction (RSF) framework is a parametrisation of transient frictional responses that is increasingly used to describe basal friction [16,24,25]. In the RSF framework, the detailed characteristics of the basal dynamics are encoded in a single state variable Θ, which evolves in response to changes in forcing over time towards a new steady value, leading to temporal lag in the system. Our two-phase model similarly introduces a time lag between the forcing and deformation due to the timescale of the porosity response. This similarity between the two systems leads to the interpretation of the porosity structure as a state variable. Indeed, [25] explicitly set the mean porosity of the till to be a function of Θ. Likewise, a comparison of the predictions between the two models may lend physical meaning to the other parameters of the RSF model.

In the RSF model, the friction coefficient $\mu = \tau_b/N$ is given by the functional form

$$\mu = \mu_0 + a \ln\left(\frac{u_b}{u_0}\right) + b \ln\left(\frac{u_0 \Theta}{D_c}\right), \tag{4.1}$$

where u_b is the sliding speed, and Θ is a state variable that contains within it all the information about the state of the bed [46]. In steady state $\Theta = D_c/u_b$, and μ_0 is the value of μ at a reference speed u_0. The parameter a controls the initial "direct" response of μ to a change in sliding speed, while $a - b$ parametrizes the eventual change once the system has re-equilibrated.

In steady state, the friction coefficient

$$\mu = \mu_0 + (a - b) \ln\left(\frac{u_b}{u_0}\right) \tag{4.2}$$

qualitatively similar to

$$\mu = \mu_1 + (3\eta\mu_1 \Delta\rho \, g\phi_m M^2 u_b/N_0^2)^{1/3} \tag{4.3}$$

for granular till, as the friction coefficient increases sub-linearly with sliding speed if $a - b > 0$. This parallel is also noted in [7].

Different evolution equations for Θ are found in the literature [46], either taking the form of an aging law,

$$\frac{d\Theta}{dt} = 1 - \left(\frac{u_b\Theta}{D_c}\right)^p, \tag{4.4}$$

or a slip law,

$$\frac{d\Theta}{dt} = -\frac{u_b\Theta}{D_c}\ln\left(\frac{u_b\Theta}{D_c}\right). \tag{4.5}$$

While similar to the two-phase model in that the transient adjustment of the state of the bed alters the drag away from the steady-state drag law, leading to initial strengthening before steady conditions are recovered over longer timescales, we now have timescale of adjustment of D_c/u_b, which decreases with increasing sliding speed, in contrast to the two-phase model.

Further differences emerge in the predictions of the two models when considering the finer details of the time-evolution of the friction. If we once more consider the response of this system to a small periodic change in N of the form $\bar{N} + \Delta N e^{-i\omega t}$ and observe the response in u_b, we may compare the resultant time-dependent sliding law to our two-phase model results. Both the aging and slip law for Θ reduce to the same linearised form,

$$i\omega\hat{\Theta} = \frac{\hat{u}}{u_b} + \frac{\hat{\Theta}u_b}{D_c}, \tag{4.6}$$

so

$$\hat{\mu} = \left(a + \frac{b}{i\omega D_c/u_b - 1}\right)\frac{\hat{u}}{u_b}. \tag{4.7}$$

If τ_b is held fixed then

$$\hat{u} = -\frac{u_b\tau_b}{\bar{N}^2}\frac{1 - i\omega D_c/u_b}{a - b - i\omega a D_c/u_b}\Delta N e^{-i\omega t} = \frac{1 - i\omega D_c/u_b}{1 - \frac{a}{a-b}i\omega D_c/u_b}\frac{du_b}{dN}\Delta N e^{-i\omega t}, \tag{4.8}$$

and the amplitude A and phase lag θ are given by

$$Ae^{i\theta} = \frac{1 - i\omega D_c/u_b}{1 - \frac{a}{a-b}i\omega D_c/u_b}. \tag{4.9}$$

As in the two-phase model, at low frequencies the steady sliding law is recovered, with $A \to 1$ and $\theta \to 0$. However, the phase lag decays with $\theta \sim \omega$ (rather than $\sqrt{\omega}$ as in the two-phase model) as the frequency of the forcing decreases. The time lag tends to a constant D_c/u_b rather than continuing to increase with the period of the forcing.

Another difference is that the presence of a direct effect ($a \neq 0$) means there is always an instantaneous response ($\theta = 0$) at high frequencies, with a relative amplitude $A = 1 - b/a$ that does not decay to 0 as ω increases, in contrast to the two-phase model. The maximal phase lag occurs instead on intermediate timescales at a value of $\theta = \arctan(b/2\sqrt{a(a-b)})$. While this can be made to match the $\pi/4$ of the two-phase model if $a = (1 + \sqrt{2})b/2$, the behaviour of the RSF system at rapid forcing frequencies of oscillation is very different.

Time-dependent experiments measuring the amplitude and lag of the velocity response, over a wide range of forcing frequencies, could be performed on granular till to determine which of these models provides the better fit. Very rapid oscillations can be used to measure the magnitude of the instantaneous effect, similar to the results of [16], while very slow oscillations show the recovery towards steady state and would allow for a robust measure of the phase lag between the forcing and response. [47] performed a set of oscillatory experiments for the analogous case of ice-on-rock friction and observed both an increase in amplitude with increasing period and noted a lag in the frictional response, interpreted through the view of a RSF model fitted per run.

The dependence of the lag on frequency is an experimentally tractable way to test the validity of the two models. While rate-and-state provides a convenient reduction of the variable space, it is important to note that some information about the physics is lost in the process, and interrogate to what extent this affects the resulting sliding laws if one representative value of the governing parameters is chosen.

(c) Coupling with ice dynamics

In this analysis, we have imposed a (time-dependent) effective pressure at the ice-till interface. Since this causes the till to dilate and compact, the volume of water in the till is not fixed - we have assumed that a sufficient source of water is available at the surface of the till as required, making this a drained model. Conservation of mass and till dilatancy determines the volume of water needed to enter the pore space to produce this change in effective pressure. From our simulations (figures 4c and 5c), 2mm of water per unit surface area are required over a scale of hours, implying a very modest induced flowrate even in the relatively high-permeability situation illustrated. We could instead choose to impose the changes in water content, and calculate the resulting pressure fluctuations - this is the undrained configuration. In this way, we could couple our till model to a parametrisation of melt and refreezing occurring at the base of the ice, as in the model of [48], where the water availability in the till depends on the sliding speed of the ice.

Indeed, an exciting potential extension to this work more generally is the dynamic coupling between the deformation of the ice and the till, since in this paper we have assumed that the role of the ice is to provide a constant basal traction and normal stress on the till surface, as this is usually the boundary condition applied in ring-shear tests [28]. However, for the large scale deformation of ice sheets, the basal sliding speed is a key control on the total ice flux and thus over long timescales will alter the thickness of the ice above, and in turn set both the ice overburden pressure (directly proportional to ice depth) and basal shear stress (gradients in surface height). This coupling [25] could be important for the long term evolution of ice streams, in particular in response to a pulse of meltwater (such as a lake-drainage event) or the start of a surge, or in response to the rapid disintegration of an ice-shelf.

Finally, there is the important question of the coupling between the base of the ice and the surface of the till. While here we have examined the response of the till to the conditions at its surface, the presence of a layer of water between ice and bed may effectively decouple the two. As the ice approaches floatation, we would expect an increasing degree of slip between the ice and till, so that the basal motion of the ice is not fully transmitted to the till. This could lead to a non-monotonic till flux relationship with pressure such as observed in [49]. Given the importance of understanding till fluxes when explaining the formation of subglacial bedforms, an extension to this work would be to consider the three-layer system that incorporates an increasingly deep film of water at the ice-till interface to more fully understand the transition from deep till deformation to sliding over a water-filled cavity.

5. Conclusion

We have described a modelling framework for the coupled flow of water through, and the deformation of, water-saturated subglacial till, starting from physically-based mass and force balance equations describing the motion of both water and till. Using this model we have shown that shear dilation, when coupled to the flow of water into the changing pore space, induces large pressure fluctuations which modulate the normal stress felt by the till, and hence its ability to deform. We find behaviour such as transient dilatant strengthening appearing as emergent phenomena of the model. We show this behaviour in both the general formulation and implementing a granular rheology for the till.

The transient flows induced by dilation and compaction of till significantly alter the deformation rate and depth of shear away from their steady-state values. This suggests both basal sliding rates and till transport may be poorly represented by current parametrisations which only

depend on instantaneous effective pressure. Instead, in the case of fluctuating water pressure, we predict long-lasting continued shear at depth, followed by dilatant strengthening, altering the deformation rate and till flux. Accurately quantifying the link between till rheology, ice dynamics, and subglacial sediment discharge influences our understanding of glacially driven erosion and mechanisms of bedform construction. Since we are able to calculate analytic expressions for the modified time-dependent sliding laws in the case of small amplitude periodic forcing, these could be included in large-scale ice sheet models.

Till is a complex material and characterising its behaviour requires a combination of careful laboratory, field, and theoretical approaches. Here we have shown the potential for continuum wet granular mechanics to capture both steady shearing and the transient coupling between water pressure, till deformation, and porosity variations. In particular, we highlight shear-dilatancy as an important mechanism driving the decreased diffusivity of effective pressure through subglacial till, leading to a persistent transient response. However, our quantitative results rely on parameters that currently lack experimental constraint, suggesting the importance of further experiments, especially in the case of fluctuating effective pressure that may be most relevant to glaciers over the daily cycle of melt or tides. Grain-scale simulations can also provide quasi-experimental data, but our results highlight the need to accurately account for water flow to produce results that are strikingly different to a dry granular till.

References

1. Bamber JL, Vaughan DG, Joughin I. 2000 Widespread Complex Flow in the Interior of the Antarctic Ice Sheet. *Science* **287**, 1248–1250.
2. Anandakrishnan S, Blankenship DD, Alley RB, Stoffa PL. 1998 Influence of subglacial geology on the position of a West Antarctic ice stream from seismic observations. *Nature* **394**, 62–65.
3. Tulaczyk S, Kamb WB, Engelhardt HF. 2000 Basal mechanics of Ice Stream B, west Antarctica: 1. Till mechanics. *Journal of Geophysical Research: Solid Earth* **105**, 463–481.
4. Clarke GK. 2005 Subglacial Processes. *Annual Review of Earth and Planetary Sciences* **33**, 247–276.
5. Iverson NR, Hooyer TS, Baker RW. 1998 Ring-shear studies of till deformation: Coulomb-plastic behavior and distributed strain in glacier beds. *Journal of Glaciology* **44**, 634–642.
6. Iverson NR. 2010 Shear resistance and continuity of subglacial till: hydrology rules. *Journal of Glaciology* **56**, 1104–1114.
7. Kamb B. 1991 Rheological nonlinearity and flow instability in the deforming bed mechanism of ice stream motion. *Journal of Geophysical Research: Solid Earth* **96**, 16585–16595.
8. Padman L, Siegfried MR, Fricker HA. 2018 Ocean Tide Influences on the Antarctic and Greenland Ice Sheets. *Rev. of Geophys.* **56**, 142–184.
9. Smith LC, Andrews LC, Pitcher LH, Overstreet BT, Rennermalm AK, Cooper MG, Cooley SW, Ryan JC, Miège C, Kershner C, Simpson CE. 2021 Supraglacial River Forcing of Subglacial Water Storage and Diurnal Ice Sheet Motion. *Geophysical Research Letters* **48**, e2020GL091418. e2020GL091418 2020GL091418.
10. Sundal AV, Shepherd A, Nienow P, Hanna E, Palmer S, Huybrechts P. 2011 Melt-induced speed-up of Greenland ice sheet offset by efficient subglacial drainage. *Nature* **469**, 521–524.
11. Bindschadler RA, Vornberger PL, King MA, Padman L. 2003 Tidally driven stick-slip motion in the mouth of Whillans Ice Stream, Antarctica. *Ann. Glaciol.* **36**, 263–272.
12. Engelhardt H, Kamb B. 1997 Basal hydraulic system of a West Antarctic ice stream: constraints from borehole observations. *Journal of Glaciology* **43**, 207–230.

13. Doyle SH, Hubbard B, Christoffersen P, Law R, Hewitt DR, Neufeld JA, Schoonman CM, Chudley TR, Bougamont M. 2021 Water flow through sediments and at the ice-sediment interface beneath Sermeq Kujalleq (Store Glacier), Greenland. *Journal of Glaciology* p. 1–20.

14. Damsgaard A, Goren L, Suckale J. 2020 Water pressure fluctuations control variability in sediment flux and slip dynamics beneath glaciers and ice streams. *Communications Earth & Environment* **1**, 66.

15. Damsgaard A, Egholm DL, Beem LH, Tulaczyk S, Larsen NK, Piotrowski JA, Siegfried MR. 2016 Ice flow dynamics forced by water pressure variations in subglacial granular beds. *Geophysical Research Letters* **43**, 12,165–12,173.

16. Zoet LK, Iverson NR, Andrews L, Helanow C. 2021 Transient evolution of basal drag during glacier slip. *Journal of Glaciology* p. 1–10.

17. Joughin I, Smith BE, Schoof CG. 2019 Regularized Coulomb Friction Laws for Ice Sheet Sliding: Application to Pine Island Glacier, Antarctica. *Geophysical Research Letters* **46**, 4764–4771.

18. Brondex J, Gagliardini O, Gillet-Chaulet F, Durand G. 2017 Sensitivity of grounding line dynamics to the choice of the friction law. *Journal of Glaciology* **63**, 854–866.

19. Moore PL, Iverson NR. 2002 Slow episodic shear of granular materials regulated by dilatant strengthening. *Geology* **30**, 843–846.

20. Pailha M, Pouliquen O. 2009 A two-phase flow description of the initiation of underwater granular avalanches. *Journal of Fluid Mechanics* **633**, 115–135.

21. Jop P, Forterre Y, Pouliquen O. 2006 A constitutive law for dense granular flows. *Nature* **441**.

22. Boyer F, Guazzelli E, Pouliquen O. 2011 Unifying Suspension and Granular Rheology. *Phys. Rev. Lett.* **107**, 188301.

23. Baumgarten AS, Kamrin K. 2019 A general fluid-sediment mixture model and constitutive theory validated in many flow regimes. *Journal of Fluid Mechanics* **861**, 721–764.

24. Lipovsky BP, Dunham EM. 2017 Slow-slip events on the Whillans Ice Plain, Antarctica, described using rate-and-state friction as an ice stream sliding law. *Journal of Geophysical Research: Earth Surface* **122**, 973–1003.

25. Minchew BM, Meyer CR. 2020 Dilation of subglacial sediment governs incipient surge motion in glaciers with deformable beds. *Proceedings of the Royal Society A: Mathematical, Physical and Engineering Sciences* **476**, 20200033.

26. Rathbun AP, Marone C. 2010 Effect of strain localization on frictional behavior of sheared granular materials. *Journal of Geophysical Research: Solid Earth* **115**.

27. Boulton GS, Hindmarsh RCA. 1987 Sediment deformation beneath glaciers: Rheology and geological consequences. *Journal of Geophysical Research: Solid Earth* **92**, 9059–9082.

28. Zoet LK, Iverson NR. 2020 A slip law for glaciers on deformable beds. *Science* **368**, 76–78.

29. Fowler AC. 2010 The formation of subglacial streams and mega-scale glacial lineations. *Proceedings of the Royal Society A: Mathematical, Physical and Engineering Sciences* **466**, 3181–3201.

30. Rosier SHR, Gudmundsson GH, Green JAM. 2015 Temporal variations in the flow of a large Antarctic ice stream controlled by tidally induced changes in the subglacial water system. *Cryosphere* **9**, 1649–1661.

31. Amarsid L, Delenne JY, Mutabaruka P, Monerie Y, Perales F, Radjai F. 2017 Viscoinertial regime of immersed granular flows. *Phys. Rev. E* **96**, 012901.

32. Kasmalkar I, Damsgaard A, Goren L, Suckale J. 2021 Shear Variation at the Ice-Till Interface Changes the Spatial Distribution of Till Porosity and Meltwater Drainage. *Journal of Geophysical Research: Earth Surface* **126**, e2021JF006460. e2021JF006460 2021JF006460.

33. Wang X, Li G, Liu Q. 2022 An updated critical state model by incorporating inertial effects for granular material in solid–fluid transition regime. *Granular Matter* **24**, 38.

34. Boulton GS, Dobbie KE. 1998 Slow flow of granular aggregates: the deformation of sediments beneath glaciers. *Philosophical Transactions of the Royal Society of London. Series A: Mathematical, Physical and Engineering Sciences* **356**, 2713–2745.

35. Iverson NR, Hooyer TS, Fischer UH, Cohen D, Moore PL, Jackson M, Lappegard G, Kohler J. 2007 Soft-bed experiments beneath Engabreen, Norway:regelation infiltration, basal slip and bed deformation. *Journal of Glaciology* **53**, 323–340.

36. Freeze RA, Cherry JA. 1979 *Groundwater*. Upper Saddle River, NJ 07458: Prentice Hall, Inc.

37. Minchew BM, Simons M, Riel B, Milillo P. 2017 Tidally induced variations in vertical and horizontal motion on Rutford Ice Stream, West Antarctica, inferred from remotely sensed observations. *J. Geophys. Res. Earth Surface* **122**, 167–190.

38. Gudmundsson GH. 2006 Fortnightly variations in the flow velocity of Rutford Ice Stream, West Antarctica. *Nature* **444**, 1063–1064.

39. Robel AA, Tsai VC, Minchew B, Simons M. 2017 Tidal modulation of ice shelf buttressing stresses. *Annals of Glaciology* **58**, 12–20.

40. Rosier SHR, Gudmundsson GH. 2020 Exploring mechanisms responsible for tidal modulation in flow of the Filchner–Ronne Ice Shelf. *The Cryosphere* **14**, 17–37.

41. Warburton KLP, Hewitt DR, Neufeld JA. 2020 Tidal Grounding-Line Migration Modulated by Subglacial Hydrology. *Geophysical Research Letters* **47**, e2020GL089088. e2020GL089088 10.1029/2020GL089088.

42. Iken A, Bindschadler RA. 1986 Combined measurements of Subglacial Water Pressure and Surface Velocity of Findelengletscher, Switzerland: Conclusions about Drainage System and Sliding Mechanism. *Journal of Glaciology* **32**, 101–119.

43. Riel B, Minchew B, Bischoff T. 2021 Data-Driven Inference of the Mechanics of Slip Along Glacier Beds Using Physics-Informed Neural Networks: Case Study on Rutford Ice Stream, Antarctica. *Journal of Advances in Modeling Earth Systems* **13**, e2021MS002621. e2021MS002621 2021MS002621.

44. Guerin G, Mordret A, Rivet D, Lipovsky BP, Minchew BM. 2021 Frictional Origin of Slip Events of the Whillans Ice Stream, Antarctica. *Geophysical Research Letters* **48**, e2021GL092950. e2021GL092950 2021GL092950.

45. Sergienko OV, MacAyeal DR, Bindschadler RA. 2009 Stick–slip behavior of ice streams: modeling investigations. *Annals of Glaciology* **50**, 87–94.

46. van den Ende M, Chen J, Ampuero JP, Niemeijer A. 2018 A comparison between rate-and-state friction and microphysical models, based on numerical simulations of fault slip. *Tectonophysics* **733**, 273–295. Physics of Earthquake Rupture Propagation.

47. McCarthy C, Skarbek RM, Savage HM. 2022 Tidal Modulation of Ice Streams: Effect of Periodic Sliding Velocity on Ice Friction and Healing. *Frontiers in Earth Science* **10**.

48. Tulaczyk S, Kamb WB, Engelhardt HF. 2000 Basal mechanics of Ice Stream B, west Antarctica: 2. Undrained plastic bed model. *Journal of Geophysical Research: Solid Earth* **105**, 483–494.

49. Hansen DD, Zoet LK. 2022 Characterizing Sediment Flux of Deforming Glacier Beds. *Journal of Geophysical Research: Earth Surface* **127**, e2021JF006544. e2021JF006544 2021JF006544.